ISSN: 2688-8645

Preliminary Design Study on the Thermal System of an Adiabatic Compressed Air Energy Storage System

Chengbin Shi*, Jingming Liao, Yaosen Chen and Feng Wang

Power China Fujian Electric Power Engineering Co., Ltd., Fuzhou 350003, China

Abstract

Compressed air energy storage (CAES) system is a new type of energy storage system with characteristics of long-term performance, high efficiency, and safety. In recent years, adiabatic CAES technology has attracted extensive attention. In this paper, the thermal models and the solution processes of the CAES system are proposed, which are verified by the design and operating data of the adiabatic CAES project in Jintan, Jiangsu province. And then, according to the comparison of different CAES technology routes, this paper selects the 300MW medium temperature CAES system with rock cavern for analysis. With the project in Yongchun, Fujian province as an example, the optimal scheme is to select the expander inlet pressure of 17MPa and the inlet pressure variation range of 6MPa, and the thermodynamic processes and technical parameters of this scheme are analyzed. According to the analysis above, a preliminary design plan is obtained.

Keywords

Compressed Air Energy Storage; Adiabatic; 300MW; Medium Temperature; Design.

1. Introduction

Compressed air energy storage (CAES) technology, which can mitigate the impact of renewable energy and regulate peak load on the power grid, is considered to be one of the most promising energy storage technologies [1]. CAES technology is a new type of energy storage technology, which is characterized by high safety, large energy storage scale, long discharge time, long service life, flexible location, clean and efficient [2]. CAES can be classified as D(diabatic)-, A(adiabatic)-, I(isothermal)-CAES by their idealized change of state [3]. In recent years, universities, research institutes and enterprises have attached great attention to the development and application of CAES. At present, the large CAES power stations put into commercial operation in the world are Huntorf power station in Germany and McIntosh power station in the United States, both of which adopt the traditional natural gas afterburning mode, and the actual operation efficiency is low [4, 5]. In recent years, organizations in China are working to promote the application of A-CAES technology. The physical simulation system of CAES named TICC-500 had been built in Wuhu, Anhui province since 2014. After that, with the technology support of Chinese Academy of Sciences, the 10MW verification platform of CAES in Bijie, Guizhou province and the 10MW (Phase I) peak-shaving power station of CAES in Feicheng, Shandong province had been put into operation in 2021, and the 100MW CAES project in Zhangbei, Hebei province had been put into the commissioning stage in 2022. With the technical support of Tsinghua University, the 100kW solar power composite CAES industrial demonstration project in Xining, Qinghai province had been put into operation in 2016, and the CAES project in Jintan, Jiangsu province had been put into commercial operation in May 2022 [6]. In addition, the feasibility study of CAES projects such as Feicheng (Phase II) 300MW, Pingdingshan (200MW), Tai'an (300MW), Yingcheng (300MW), Chaoyang (300MW), Yongchun (300MW) has been completed recently.

ISSN: 2688-8645

In recent years, major research directions focus on improving the performance and conversion efficiency of CAES system. Different research models and methods have been put forward. Mazloum Y et al. discussed the impact of different heat storage devices in CAES on energy consumption and efficiency, and found that using a quartzite packed bed can improve the system efficiency to 70.1% [7]. Sciacovelli et al. proposed a system model that simulated the operation of CAES and evaluated the impact of thermal energy storage (TES) systems integrated into CAES systems on the overall system performance, and the results showed that when the TES system operated at a storage efficiency of more than 90%, the CAES system achieved an efficiency of 60% to 70% [8]. Hamidreza Mozayeni et al. studied real-time system dynamics models and achieved the results that system operating parameters had significant impact on the system, such as compressor intake flow, expander intake flow, and air storage pressure, therefore, it was necessary to select appropriate air flow mass based on actual conditions to ensure system performance [9]. Guo Huan et al. established a thermal system model for CAES, and analyzed the cause and effect of the system efficiency and factors such as pressure ratio distribution, compression stages, and heat exchanger (HX) efficiency [10]. Wen Xiankui et al. established a CAES model using Aspen Plus software, and studied the relationship between system efficiency and air inlet parameters [11]. Han Zhonghe et al. established an analytical model for CAES and proposed a CAES structure with high energy storage density and heat storage efficiency [12].

However, to the author's knowledge, little literature recorded the modeling and design process of the CAES system, especially the large-scale A-CAES thermal system. Generally, the A-CAES thermal system contains the compressor, the expander, the heat exchangers, the heat storage tanks and the air storage chamber, the dynamic process of which affects the system performance greatly. In this paper, the simulation models and solution processes of the A-CAES thermal system are proposed, which is verified by the design and operation parameters of the Jintan project. Then the comparison and selection of different CAES technology routes is carried out. With the project in Yongchun, Fujian province as an example, the technical parameters are analyzed, and the preliminary design scheme of the CAES thermal system is obtained.

2. Mathematical Model and Solution Process

As shown in Figure 1. When the power grid operates at low load state, the CAES system absorbs excess electric energy from the power grid and drives the compressor to work, compressing the low-pressure air into high-pressure air and storing it in the air storage chamber. The heat generated during the charging process is transferred through the heat exchange system and stored in the heat storage unit. When the power grid operates at peak load condition, the high-pressure air in the air storage chamber of the CAES system is released and enters the expander to generate electricity. During the operation of the expander, the heat stored in the heat storage unit is transferred to the air through the heat exchange system.

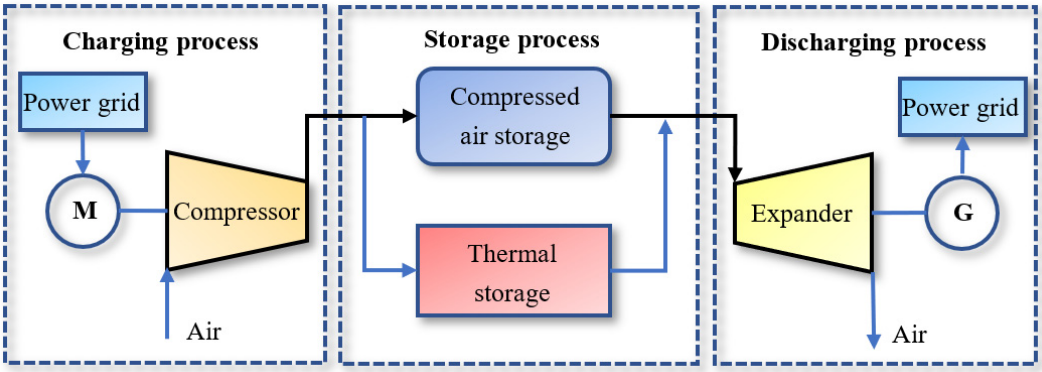

Figure 1. Schematic diagram of A-CAES system.

ISSN: 2688-8645

2.1. Thermal System Modeling

2.1.1. Governing Equations

According to the inlet and outlet temperature of the compressor, the pressure ratio can be calculated in Eq (1).

$$\varepsilon_{c\_i} = e^{\frac{m_i}{m_i-1}(\ln T_{c\_out\_i} - \ln T_{c\_in\_i})} \tag{1}$$

where e is the natural logarithm; subscript c represents the compressor. subscript out represents the outlet data; subscript in represents the inlet data; subscript c_i represents ith compressor cylinder; ε_{c_i} represents the pressure ratio of i th compressor cylinder; m_i represents the polytropic exponent of i th compressor cylinder; $T_{c\_in\_i}$ represents the inlet temperature of i th compressor cylinder; $T_{c\_out\_i}$ represents the outlet temperature of i th compressor cylinder.

The outlet pressure of the compressor can be calculated in Eq. (2).

$$p_{c\_out\_i} = \varepsilon_{c\_i} p_{c\_in\_i} \tag{2}$$

where $p_{c\_out\_i}$ represents the outlet pressure of ith compressor cylinder; $p_{c\_in\_i}$ represents the inlet pressure of ith compressor cylinder.

The shaft power of the compressor can be calculated in Eq. (3).

$$W_{c\_d\_i} = \frac{m_i}{m_i-1} R T_{c\_in\_i} \left(\varepsilon_{c\_i}^{\frac{m_i-1}{m_i}} - 1 \right) / \eta_{d\_i} \tag{3}$$

where $W_{c\_d\_i}$ represents the shaft power of i th compressor cylinder; R represents the gas constant of air; η_{d_i} represents the polytropic compression efficiency of i th compressor cylinder.

The actual power consumption of the compressor can be calculated in Eq. (4).

$$W_{c\_i} = \frac{W_d}{\eta_{c\_d}} \tag{4}$$

where W_{c_i} represents the actual power consumption of i th compressor cylinder; η_{c_d} represents the electric efficiency of ith compressor cylinder.

The total power consumption of the compressor can be calculated in Eq. (5).

$$W_c = \sum_{i=1}^{n} W_{c\_i} \tag{5}$$

where n represents the number of compressor cylinders.

The flow rate of heat storage medium in ith compressor side HX can be calculated as Eq. (6).

$$q_{c\_w\_i} = \left(h_{hx\_a\_in\_i} - h_{hx\_a\_out\_i}\right) q_{c\_a} \eta_{hx} / \left(h_{hx\_w\_out\_i} - h_{hx\_w\_in\_i}\right) \tag{6}$$

The flow rate of heat storage medium in ith expander side HX can be calculated in Eq. (7).

$$q_{t\_w\_i} = \left(h_{hx\_a\_in\_i} - h_{hx\_a\_out\_i}\right) q_{t\_a} / \left[\left(h_{hx\_w\_out\_i} - h_{hx\_w\_in\_i}\right) \eta_{hx}\right] \tag{7}$$

The output power of ith expander cylinder can be calculated in Eq. (8).

$$W_{t\_i} = \left(h_{t\_out\_i} - h_{t\_in\_i}\right) q_{t\_a} \eta_{t\_i} \tag{8}$$

where W_{t_i} represents the output power of ith expander cylinder; $h_{t\_out\_i}$ represents the outlet enthalpy of the air in ith expander cylinder; $h_{t\_in\_i}$ represents the inlet enthalpy of the air in ith expander cylinder; q_{t_a} represents the flow rate of the air in i th expander cylinder; η_{t_i} represents the electric efficiency of ith expander cylinder.

The total output power of the expander can be calculated in Eq. (9).

$$W_t = \sum_{i=1}^{n} W_{t\_i} \tag{9}$$

where n represents the number of expander cylinders.

ISSN: 2688-8645

2.1.2. Boundary Conditions

Boundary conditions of thermal system in this study can be expressed in Eqs. (10) - (12). The inlet temperature and pressure of air in the first compressor cylinder is according to the atmospheric environment during the charging process, while the outlet pressure of air in the last expander cylinder is according to the back pressure of atmospheric environment during the discharging process.

$$T_{c\_in\_1} = T_{air} \tag{10}$$

$$P_{c\_in\_1} = P_{air} \tag{11}$$

$$P_{t\_out\_n} = P_{air} \tag{12}$$

2.1.3. Solution Process

The solution flowchart of the CAES thermal system is shown in Figure 2.

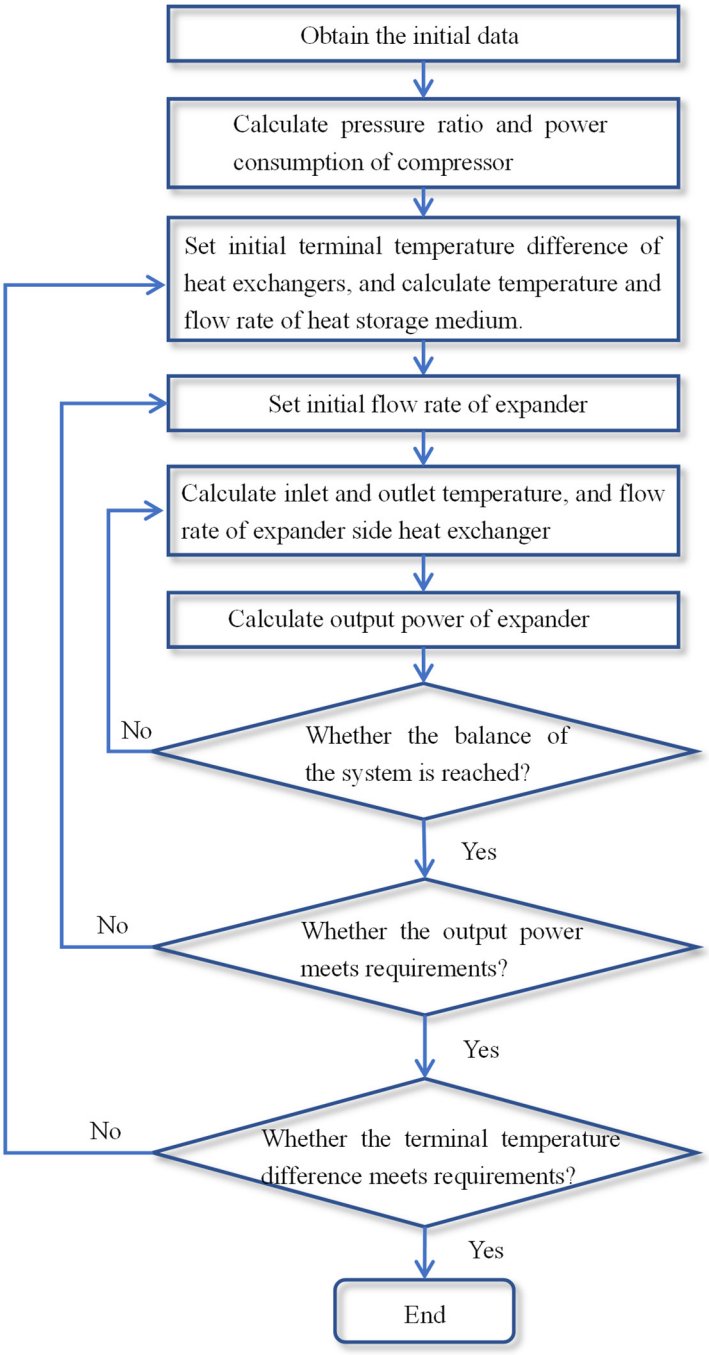

Figure 2. Flow chart of the solution process of the CAES thermal system.

ISSN: 2688-8645

In the First step, the initial parameters, including the temperature, air pressure and humidity of the atmospheric environment, are obtained based on local hydrological and meteorological data. The second step is to calculate the initial parameters of the compressor including pressure ratio and power consumption based on environmental parameters. The third step is to assume the initial end difference of the compressor side heat exchangers, and calculate the temperature, pressure, and other parameters of the heat storage medium based on the end difference of the compressor side heat exchangers. Step 4 is to assume the initial air flow rate of the expander. Step 5 is to set the initial heat transfer end difference of the expander, while calculate the flow rate, inlet and outlet temperature, and pressure parameters of the expander side heat exchangers based on the previously assumed data. Step 6 is to calculate the output power of the expander. Step 7 is to compare the heat and compressed air generated during the compression process with the heat and compressed air consumed during the expansion process to determine whether the system has reached equilibrium. If the system has reached equilibrium, continue the next step. If the system has not reached equilibrium, return to step 5. Step 8 is to determine whether the output data of the compressed air energy storage system has reached the set value. If the output data has reached the set value, continue the next step. If the output data has not reached the set value, return to step 4. Step 9 is to determine whether the assumptive end difference of heat exchangers is reasonable. If it is reasonable, end the calculation. If it is not reasonable, return to step 3.

2.2. Thermodynamic Process Calculation and Volume Estimation of the Cavern

2.2.1. Governing Equations

Differential equation of the air in the gas storage cavern can be expressed in Eq. (13).

$$Vd\left(\rho c_p T\right) + Ak(T - T_w)dt = amc_p T_{in} dt \tag{13}$$

where V represents the volume of the gas storage cavern; ρ represents the density of the air in the rock cavern; c_p represents the specific heat capacity of the air in the rock cavern; T represents the temperature of the air in the rock cavern; T_{in} represents the temperature of the air entering the rock cavern; A represents the heat exchange area of the rock cavern; k represents the heat exchange coefficient between the air and the surface of the rock cavern; T_w the wall temperature of the rock cavern. m represents the air flow rate entering the rock cavern; a represents the operating status of the CAES system; In charging conditions, a=1; in discharging conditions, a=-1; and in storage conditions, a=0.

State equation of the air in the rock cavern can be expressed in Eq. (14).

$$P = Z\rho RT \tag{14}$$

where Z is the compressibility factor, and P represents the pressure of the air in the rock cavern.

Differential equation of the thermal conductivity of the rock mass can be expressed in Eq. (15).

$$\frac{\partial T_R}{\partial t} = \frac{\lambda_R}{\rho_R c_R}\left(\frac{\partial^2 T_R}{\partial r^2} + \frac{1}{r}\frac{\partial T_R}{\partial r}\right) \tag{15}$$

where T_R represents the temperature of the rock mass in the rock cavern; λ_R represents the thermal conductivity of the rock mass in the rock cavern; ρ_R represents the density of the rock mass in the rock cavern; c_R represents the specific heat capacity of the rock mass in the rock cavern; r represents the equivalent radius of the rock cavern.

The volume of the rock cavern can be calculated in Eq. (16).

$$V = \frac{\int_{t_0}^{t_1} m(t)dt}{P_1/RT_1 - P_0/RT_0} \tag{16}$$

where V represents the initial gas storage volume of the rock cavern; m(t) represents the flow rate of the exhaust air in the compressor during the charging process; t_0 represents the start time of the charging condition; t_1 represents the end time of the charging condition; P_0 represents the air pressure of the rock cavern at the beginning of the charging condition; P_1

ISSN: 2688-8645

represents the air pressure of the rock cavern at the end of the charging condition; T_0 represents the air temperature of the rock cavern at the beginning of the charging condition; T_1 represents the air temperature of the rock cavern at the end of the charging condition; R represents the gas constant.

2.2.2. Boundary Conditions

Boundary conditions of the rock cavern model in this study can be expressed as Eqs. (17) and (18).

$$T_R|_{r=r_{out}} = T_{out} \tag{17}$$

$$-\lambda_R \left(\frac{\partial T}{\partial r}\right)\Big|_{r=r_{in}} = k(T_w - T) \tag{18}$$

The third boundary condition is applied to calculate the heat transfer in the rock surface.

2.2.3. Solution Process

The solution flowchart of thermodynamic process calculation and volume estimation of the CAES rock cavern is shown in Figure 3.

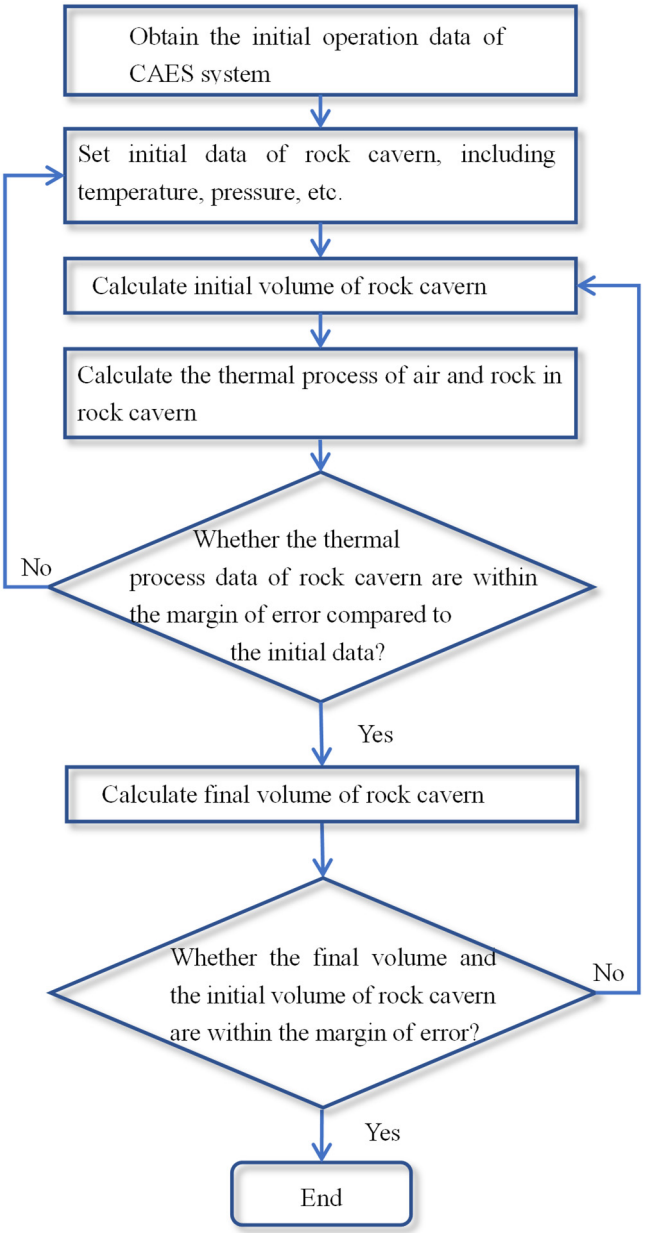

Figure 3. Flow chart of the solution process of the CAES rock cavern.

ISSN: 2688-8645

In the first step, the initial operation data of CAES system are obtained. In the second step, the initial parameters of the cavern, including the initial temperature and pressure of the cavern air, and the initial temperature of the rock are set. The third step is to calculate the initial volume of the cavern. In the fourth step, the thermodynamic process of air and rock in the cavern is calculated. Step 5 is to judge whether the parameters of the initial state and the final state calculated in the fourth step are within the error range. If they are within the error range, continue the next step. If they are not within the error range, return to the second step. Step 6 is to calculate the final volume of the cavern. Step 7 is to determine whether the initial and final cavern volumes calculated in Step 6 are within the error range. If they are within the error range, end the calculation. If they are not within the error range, return to the third step.

2.3. Verification of the Models

In this section, the mathematical models and solution methods proposed in this paper will be verified by the design and operation data of the Jintan CAES system.

As shown in Figure 4, the Jintan CAES project is a commercial power station which operates at 60MW electrical output. During the charging process, the air is compressed by three compressor cylinders respectively and inflated into the salt cavern. The compression heat is exchanged by HXs and stored. During the discharging process, the compressed air is released from the salt cavern, heated in the HXs and expanded in the expander.

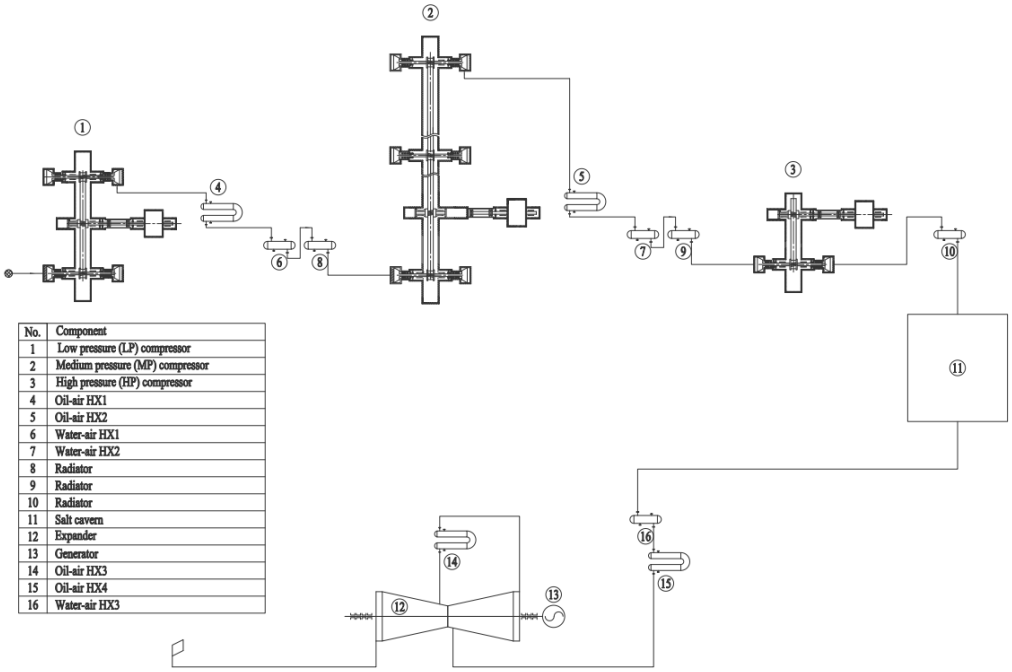

No.	Component
1	Low pressure (LP) compressor
2	Medium pressure (MP) compressor
3	High pressure (HP) compressor
4	Oil-air HX1
5	Oil-air HX2
6	Water-air HX1
7	Water-air HX2
8	Radiator
9	Radiator
10	Radiator
11	Salt cavern
12	Expander
13	Generator
14	Oil-air HX3
15	Oil-air HX4
16	Water-air HX3

Figure 4. The schematic diagram of Jintan CAES system

The main parameters of Jintan CAES system are shown in Tables 1 [6].

The comparisons of calculated value and operation value are shown in Table 2. The parameters of the power consumption of the compressor, the output power of the expander and the volume of the cavern are took into account. The comparison results show that the maximum error is 2.88% (the Shaft power consumption of the MP compressor), which demonstrate the accuracy of the calculation models.

According to the analysis above, it is worth noting that the theoretical predictions show reasonable agreement with the actual design and operating data, which verified the validity of the mathematical models and solution methods.

ISSN: 2688-8645

Table 1. The main parameters of Jintan CAES system

Parameter	Unit	Value
Inlet temperature of the LP compressor	℃	20
Inlet pressure of the LP compressor	bar	0.98
Shaft power consumption of the LP compressor	kW	26089
Inlet temperature of the MP compressor	℃	40
Inlet pressure of the MP compressor	bar	7.569
Shaft power consumption of the MP compressor	kW	23913
Inlet temperature of the HP compressor	℃	40
Inlet pressure of the HP compressor	bar	57.24
Shaft power consumption of the HP compressor	kW	8190
Inlet temperature of the HP expander	℃	300
Inlet pressure of the HP expander	MPa	12.27
Output power of the HP expander	kW	30.71
Inlet temperature of the LP expander	℃	293.5
Inlet pressure of the LP expander	MPa	1.038
Output power of the LP expander	kW	30.91
Volume of the salt cavern	10^4m^3	22.4

Table 2. Comparation of the operation value and the calculated value

Parameter	Unit	Operation value	Calculated value	error
Shaft power consumption of the LP compressor	kW	26089	25657	1.66%
Shaft power consumption of the MP compressor	kW	23913	23225	2.88%
Shaft power consumption of the HP compressor	kW	8190	8104	1.05%
Output power of the HP expander	kW	30.71	30.9	0.62%
Output power of the LP expander	kW	30.91	30.9	0.03%
Volume of the salt cavern	10^4m^3	22.4	21.97	1.92%

3. Technical Routes Selection

3.1. Selection of the Heat Storage Temperature

According to the heat storage temperature, the A-CAES systems can be classified into medium and high temperature systems [13]. Generally, the exhaust temperature of the compressor cylinders of the medium-temperature CAES systems is around 195-200 ℃, and high-pressure water is usually used as the heat storage medium. The exhaust temperature of the compressor cylinders of the high-temperature CAES systems is around 335-340 ℃, and molten salt or heat transfer oil is usually used as the heat storage medium.

The medium-temperature CAES scheme utilizes water as heat storage medium, which has the advantages of high safety, simple system operation, low operation cost and low investment. The high-temperature CAES scheme has higher system efficiency than the medium-temperature one. However, the system configuration and operation mode of high-temperature CAES system is more complex, higher investment and more operation costs than that of medium-temperature CAES system. And there is a fire hazard in the thermal oil system.

Therefore, in order to reduce the investment, while considering convenient operation and high safety, this paper recommends the technical route of the medium-temperature CAES with water as heat storage medium.

ISSN: 2688-8645

3.2. Selection of the Unit Capacity

In recent years, A-CAES systems are developing towards large-scale direction, which are shown in Table 3. It can be easily seen that the maximum capacity of the recently developed CAES systems is 300MW. Figure 5 shows a typical schematic diagram of a 300MW medium temperature A-CAES system. The compressor adopts a dual line layout, while the expander adopts a single line layout. The heat exchangers and radiators are arranged between each cylinder of the compressor to store energy and dissipate heat during the compression process. The heat exchangers are arranged between each cylinder of the expander to provide heat during the expansion process. Thus, the capacity of 300MW is selected in the following analysis.

Table 3. The progress of some A-CAES systems in China.

Project name	Capacity(MW)	Air storage type	Status
Bijie	10	Air tank	Operation
Feicheng	50	Salt cavern	Operation
Zhangjiakou	100	Air tank	Operation
Jintan	60	Salt cavern	Operation
Yingcheng	300	Salt cavern	Construction
Taian	300	Salt cavern	Construction
Chaoyang	300	Rock cavern	Planning
Yongchun	300	Rock cavern	Planning

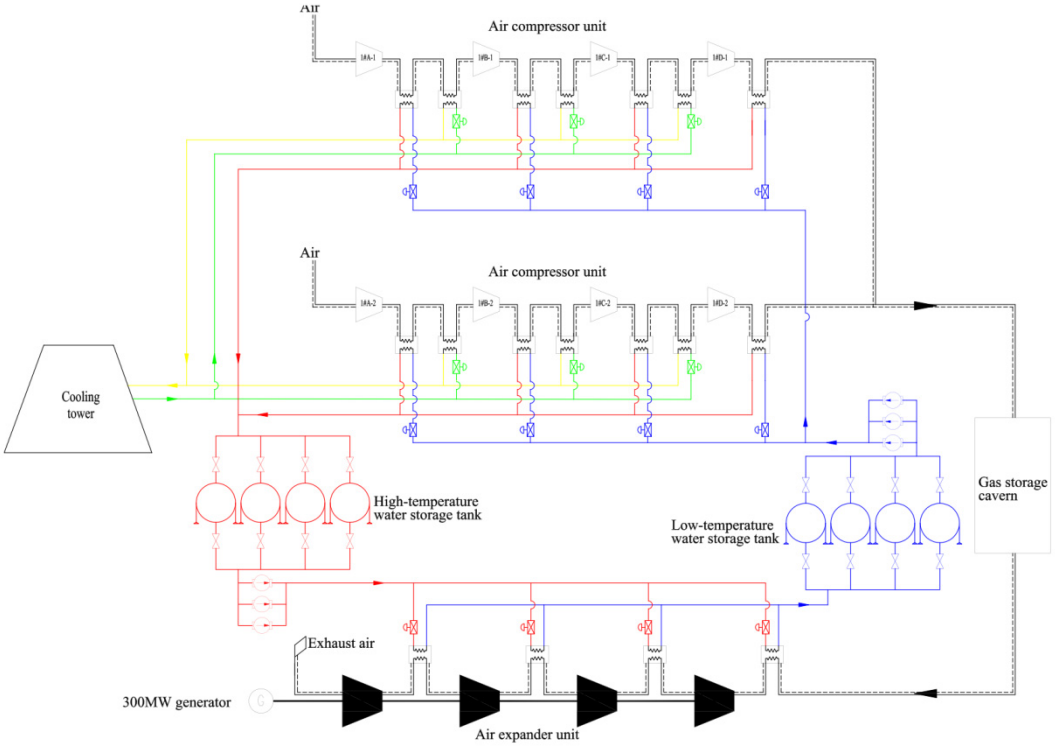

Figure 5. Schematic diagram of 300MW medium temperature A-CAES system.

3.3. Selection of the Type of the Gas Storage Chamber

The types of gas storage chambers of CAES include aboveground gas storage tanks [14], underground salt caverns [15], abandoned coal mine tunnels [16], and rock caverns [17]. The aboveground gas storage tanks are generally only suitable for small and medium-sized CAES power plants, which are mostly in the experimental stage. The unit investment of the aboveground gas storage chambers is generally higher than that of the underground gas

ISSN: 2688-8645

storage chambers. Therefore, for the perspective of economy and gas storage scale, currently projects under construction and planning mostly consider the underground gas storage scheme.

The cost of the abandoned mining caves of CAES is lower than that of the rock caverns, but the geological conditions of different mining caves vary greatly, and the possibility of uncertain engineering investment is high [18]. The cavern is the most preferable in either salt formation or hard rock. The gas storage scale of salt caverns is large with low cost, so they are widely used. But the salt caverns rely on special geographical conditions, and their operational stability needs to be demonstrated [19]. The cost of the rock caverns is higher than that of the salt caverns in the same volume, however, using rock caverns as air storage chamber of CAES can lower the limitations of special geographical conditions. Therefore, the scheme of rock cavern is analyzed in this paper.

According to the analysis above, the 300MW CAES system of medium heat storage temperature with rock cavern is analyzed in the last chapters.

4. Case Study

This paper takes the CAES system located in Yongchun, Fujian province, China as an example for subsequent analysis. The meteorological parameters are taken from the local parameters in Yongchun, Fujian province, and the parameters of the rock layer are taken from literatures [20, 21]. The input parameters of the CAES system in this study are listed in Table 4.

Table 4. Input parameters of the CAES system.

Items	Unit	Value
Annual average atmospheric temperature	℃	20.5
Annual average atmospheric pressure	kPa	94.1
Annual average atmospheric humidity	%	75.78
Number of compressor sections		4
Number of expander sections		4
Thermal storage temperature	℃	175
Initial temperature of rock in the cavern	℃	20
Thermal conductivity of rock layers	W/(m K)	100
Density of rock layers	kg/m^3	1800
Specific heat capacity of rock layers	J/(kg K)	1200
Convective heat transfer coefficient	W/(m^2 K)	60

4.1. Comparative Analysis of Schemes

For the medium temperature heat storage scheme, water is used as the heat storage medium, and the temperature of the hot water medium is about 175 ℃. Considering the pressure capacity of the rock cavern (up to 18MPa) and the pressure loss along the way from the cavern to the CAES power station, the comparison schemes are selected between the inlet pressure of the expander ranging from 15 to 17MPa and the pressure fluctuation ranging from 2 to 6MPa. The analysis is mainly conducted from the aspects of power purchase cost, manual cavern cost, and main equipment investment. The specific comparison plan is shown in Table 5.

The above comparison scheme takes Scheme 3 as the benchmark scheme and calculates the economic deviation of the other schemes from Scheme 3. According to the above comparison and selection, the required cavern volume for the pressure variation range of 4MPa and 2MPa schemes is reduced by about 100000 and 400000 cubic meters respectively than that for the pressure variation range of 6MPa, and the corresponding cavern cost is reduced by about 150 and 640 million CNY, respectively. By analyzing the impact of factors such as electricity purchase cost, cavern storage cost, and main equipment investment on the annual net income

ISSN: 2688-8645

of different schemes, this paper comprehensively consider that the Scheme 3, which has a maximum pressure of 17MPa at the expander inlet and a fluctuation range of 6MPa, is the best in the comparison schemes.

Table 5. Comparison of key parameters and annual revenue of different Schemes.

Items	unit	Scheme 1	Scheme 2	Scheme 3	Scheme 4	Scheme 5
The maximum inlet pressure of expanders	MPa	17	17	17	15	15
The expander inlet pressure fluctuation range	MPa	2	4	6	2	4
Annual electricity supply	MWh	393350.76	393350.76	393350.76	393350.76	393350.76
Annual electricity consumption	MWh	588260.50	589975.41	599262.23	586461.83	592280.84
Power supply efficiency		66.87%	66.67%	65.64%	67.07%	66.41%
The volume of rock cavern	10^4 m^3	59.64	29.75	20.06	58.83	29.66
Cost of rock cavern	10^4 CNY	+63661.72	+14873.76	Standard	+63661.72	+14873.76
Annual cost of electricity consumption	10^4 CNY	-259.55	-219.09	Standard	-301.99	-164.71
Investment of main equipment	10^4 CNY	-720	-420	Standard	-2220	-1900
Annual net income difference	10^4 CNY	-1313.99	-142.25	Standard	-1234.06	-159.64

4.2. Design and Operating Parameters

4.2.1. Design Parameters

Table 6. Parameters of the compressor cylinders.

Cylinder No.	Mass flow rate (kg/s)	Inlet pressure (barA)	Exhaust pressure (barA)	Inlet temperature (℃)	Exhaust temperature (℃)	Variable efficiency (%)	Shaft power (MW)
1	2×222.2	0.9404	4.45	20.5	195	91.8	2×41.73
2	2×222.2	4.05	14.8	40	195	91	2×36.06
3	2×222.2	14.4	50	40	195	88.2	2×35.89
4a	2×222.2	49.6	119.4	40	154	81.1	2×26.68
4b	2×222.2	49.6	177.3	40	204	86.8	2×38.40

Table 7. Parameters of the compressor side HXs.

	Items	Unit	Compressor side HX1	Compressor side HX2	Compressor side HX3	Compressor side HX4
Air side	Inlet temperature	℃	195	195	195	204/154[a]
	Outlet temperature	℃	60	60	60	60
	Inlet pressure	MPa	0.445	1.480	5.000	17.73/11.94[a]
	Mass flow rate	kg/s	2×222.2	2×222.2	2×222.2	2×222.2
Water side	Inlet temperature	℃	50	50	50	50
	Outlet temperature	℃	180	180	180	189/139[a]
	Inlet pressure	MPa	2.0	2.0	2.0	2.0
	Mass flow rate	kg/s	2×54.1	2×54.6	2×56.1	2×60.2/2×60.8[a]

note: Subscript [a] indicates the parameters at the beginning of compressor operation/at the end of compressor operation.

ISSN: 2688-8645

The calculation results are shown in Tables 6-8. The parameters of the compressor are shown in Table 6, with the No. 1-3 compressor cylinders operating at fixed frequency and the No. 4 compressor cylinder operating at variable frequency. The inlet temperature of each compressor cylinder is controlled below or equal to 40 ℃, and the exhaust temperature is controlled around 195 ℃. The variable efficiency of No. 1 and No. 2 compressor cylinders is higher than that of No. 3 and No. 4 compressor cylinders. No. 4a compressor cylinder represents the operating parameters of the fourth compressor cylinder at the beginning of operation, while No. 4b compressor cylinder represents the operating parameters of the fourth compressor cylinder at the end of operation. The design point of No. 4 compressor cylinder is at 4b working condition, and the variable efficiency continuously decreases with changes in operating pressure.

Table 8. Parameters of the expander side HXs.

	Items	Unit	Expander side HX1	Expander side HX2	Expander side HX3	Expander side HX4
Air side	Inlet temperature	℃	175	175	175	175
	Outlet temperature	℃	50	50	50	50
	Inlet pressure	MPa	2.0	2.0	2.0	2.0
	Mass flow rate	kg/s	192.5	155.3	150.6	149.3
Water side	Inlet temperature	℃	25	40	40	40
	Outlet temperature	℃	160	160	160	160
	Inlet pressure	MPa	17	4.6	1.33	0.38
	Mass flow rate	kg/s	637.4	637.4	637.4	637.4

4.2.2. Operating Parameters

The power consumption and air mass flow rate parameters of the compressor during a typical day are shown in Figure 6, with the compressor mainly operating at 0-9 hours.

The compressor operates in charging conditions, with No. 1-3 compressor cylinders operating at fixed frequency and the last cylinder of the compressor operating at variable frequency. The air mass flow rate remains almost unchanged at approximately 444.4kg/s. The power consumption of the compressor increases almost linearly over time. At the beginning of the charging condition, the compressor consumes 286.46MW of the electric power, while at the end of the charging condition, the compressor consumes 310.38MW of the electric power.

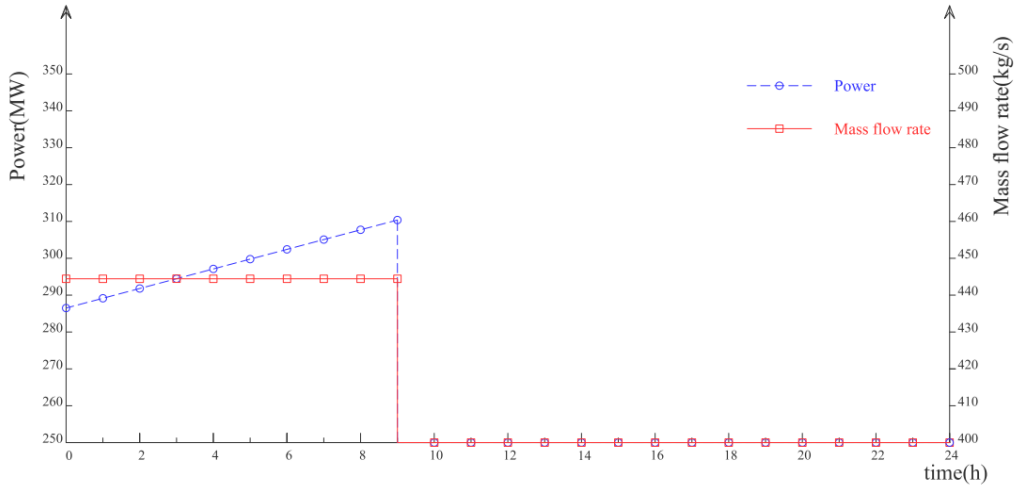

Figure 6. Operating parameters of the compressor over time during a typical day.

ISSN: 2688-8645

The output power and air mass flow rate parameters of the expander during a typical day are shown in Figure 7, with the expander mainly operating at 12-18 hours.

The expander operates under the discharging condition, and the output power of the expander remains unchanged at about 300MW during the discharging condition. In order to maintain the output power of the expander, the air mass flow rate entering the expander continuously increases due to the continuous decrease of pressure in the rock cavern during the discharging condition. The expander operates in the form of throttling and air supply. During the 12-13 hours, the expander operates in the throttling mode, and the mass flow rate remains unchanged. The inlet pressure of the expander is maintained at 15.98 MPa through throttling mode, with the air mass flow rate of 637.4 kg/s. During the 13-18 hours, as the air supply valve continues to open, the mass flow rate of air gradually increases. At 15 hours, the inlet pressure of the expander is 14.07 MPa, and the mass flow rate of air is 661.9 kg/s. At 16 hours, the inlet pressure of the expander is 13 MPa, and the mass flow rate of air is 684.5kg/s. At 18 hours, the inlet pressure of the expander is 11MPa, and the mass flow rate of air is 722.3kg/s.

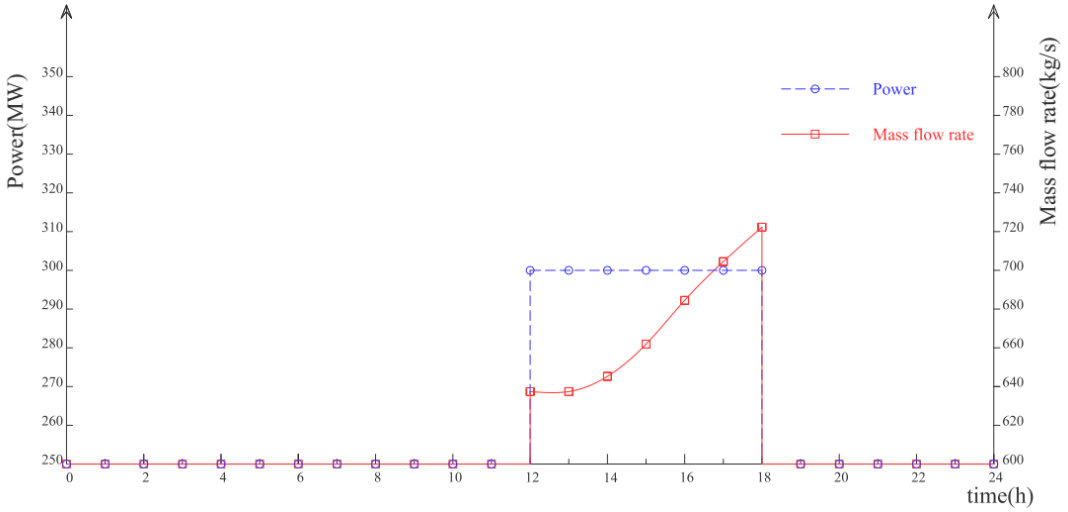

Figure 7. Operating parameters of the expander over time during a typical day.

The temperature and pressure parameters of the rock cavern in a typical day are shown in Figure 8.

During the charging process, the average temperature of the air inside the cavern gradually increases from 40 ℃ to 43.5 ℃. When the charging process is completed, the average temperature of the air inside the gas storage cavern is higher than the temperature of the rock on the wall of the gas storage cavern. There is convective heat transfer on the wall of the cavern, resulting in the decrease of 0.4 ℃ in the average temperature of the air inside the cavern during the gas storage process. At the end of the gas storage process, the average temperature of the air inside the cavern is 43.1 ℃. During the discharging process, due to gradual increase of the air mass flow rate, the average temperature of the air in the cavern decreases rapidly from 43.1 ℃ to 39.5 ℃. When the discharging process is completed, the average temperature of the air in the cavern is lower than the temperature of the rock on the wall. Therefore, due to convection heat transfer, during the storage process, the average temperature of the air in the cavern gradually increases, ultimately reaching 40 ℃.

The variation tendency of air pressure in the cavern is nearly the same with that of air temperature. However, due to thermal convection between the air and the wall of the cavern, the average pressure of the cavern is not constant during gas storage process.

ISSN: 2688-8645

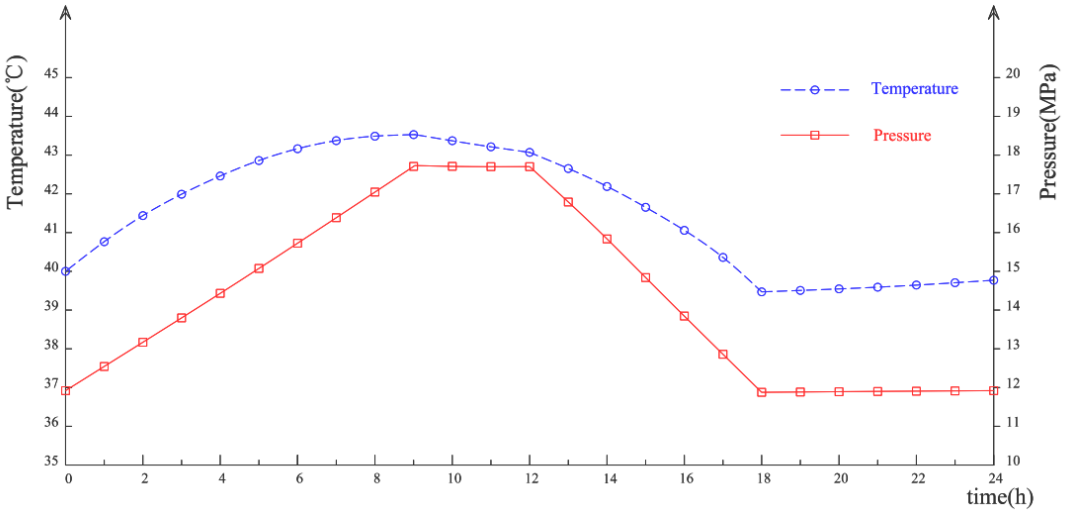

Figure 8. Operating parameters of rock cavern over time during a typical day.

4.3. Design Scheme of the CAES Thermal System

4.3.1. Air Compressor System

According to the manufacturing level, the air compressor system is designed in medium temperature scheme with dual line parallel connection and four cylinders connection in a line, with post stage cooling in each cylinder. The unit parameters are 17.73MPa/40 (20.5) ℃ /190 ℃. The No. 1-3 cylinders of the compressor adopt variable frequency starting and constant frequency operation, and the last cylinder of the compressor adopts variable frequency starting and variable frequency operation.

The compressed air from the compressor cylinders enters the heat exchangers, and exchanges heat with the medium water. After the water absorbs heat, the heat is stored in the water tanks, and the outlet air continues to enter the next stage of the compressor cylinders. After the four stages compression and multiple cooling, high-pressure air is stored in the air storage cavern, while the compression heat is stored in the water tanks.

4.3.2. Air Expander System

The air expander system is designed as a single shaft, three intermediate reheats expansion generator set with four cylinders. The unit parameters are 17MPa (a)/160 ℃/160 ℃/160 ℃ /160 ℃, and the exhaust back pressure is 0.1MPa (a).

The high-pressure air pipeline is led out from the gas storage cavern, passes through the intake heating heat exchanger, and enters the air expander. The air is led out from the exhaust outlet after expanding in the expander cylinders, heated by the reheating heat exchangers and then re-enters the next cylinders of the expander to continue expanding. At last, the low-pressure exhaust air is discharged to the atmosphere.

4.3.3. Heat Storage System

The heat storage system adopts desalinated water as the heat transfer and storage medium. The heat storage system is designed with the parameters of 2.0MPa (a) and 200 ℃. Four high-temperature spherical tanks and four low-temperature spherical tanks are set to storage water.

During the heat storage process, compressed air proceeds indirect heat exchange with cold water in air-water heat exchangers, resulting in temperature decrease of the high-temperature air and temperature increase of the cold water, completing the recovery process of compressed heat. The high-temperature water is pressurized and sent to high-temperature water storage spherical tanks for storage.

ISSN: 2688-8645

During the heat release process, the cold air released from the rock cavern and the exhaust outlet of the expander cylinders proceeds indirect heat exchange with the hot water through air-water heat exchangers. The water which has completed the heat exchange process is pressurized and sent to the low-temperature water storage spherical tanks for storage.

4.3.4. Heat Exchange System

The heat exchange system is designed to utilize the heat exchangers to absorb the compressed heat for heating air in the air expander system.

The heat exchanger adopts the shell and tube heat exchangers, with the air flowing in the tube side and the water flowing in the shell side. This project adopts four air-water heat exchangers and three air radiators on the compressor side, and four air-water heat exchangers on the expander side. The average air pressure loss of each stage of the heat exchangers is around 20kPa. The upper end difference of the air-water heat exchangers is about 15 ℃, while the lower end difference is about 10 ℃.

4.3.5. Air Storage Cavern

The rock cavern is designed as the air storage chamber while the volume is about 20.06×10^4 m^3 and the operation pressure ranges from 12MPa to 18MPa.

4.4. Conclusion

In this work, the comparison and selection of different CAES technology is carried out, and the thermal models and solution processes of CAES system and rock cavern are proposed. With the project in Yongchun, Fujian province, China as an example, the thermodynamic process and technical parameters are analyzed, and the preliminary design scheme is obtained. The following concluding remarks can be drawn:

(1). The calculation models and solution processes of the thermal system and the air storage cavern of the CAES system are proposed, which are verified by the design and operation parameters of the Jintan project.

(2). According to the comparison and selection of technical routes, the 300MW CAES technology route of medium temperature with rock cavern is selected as the research direction in this paper.

(3). Through the comparison and selection of different operating parameters, the scheme with the inlet pressure of 17MPa and the pressure variation range of 6MPa of the expander is optimal in terms of operating economy. The design and operating parameters of this scheme are described as follows.

During the charging process, the air mass flow rate of the compressor remains almost unchanged at approximately 444.4kg/s. The power consumption of the compressor increases almost linearly. At the beginning of the charging condition, the compressor consumes 286.46MW of the electric power, while at the end of the charging condition, the compressor consumes 310.38MW of the electric power. During the discharging process, the output power of the expander remains unchanged at 300MW. At the beginning of the discharging process, and the air mass flow rate of the expander remains unchanged in the throttling mode with a mass flow rate of 637.4 kg/s. At the end of discharging process, the air mass flow rate of the expander is 722.3kg/s. (4). The preliminary design scheme of the CAES thermal system, containing the air compressor system, the air expander system, the heat storage system, the heat exchange system and the air storage cavern, is obtained.

Acknowledgments

This work has been funded by the technology project of Power China Fujian Electric Power Engineering Co., Ltd. (Project number: 35-KBYZ1-2022-011).

ISSN: 2688-8645

References

[1] A. A. Solomon, D. M. Kammen, D. S. Callaway, "The role of large-scale energy storage design and dispatch in the power grid: A study of very high grid penetration of variable renewable resources," Appl. Energ. 134, 75-89 (2014).

[2] Q. Yu, Q. Wang, X. Tan et al., "A review of compressed-air energy storage," J. Renew. Sustain. Ener. 11, 042702 (2019).

[3] M. Budt, D. Wolf, R. Span et al., "A review on compressed air energy storage: Basic principles, past milestones and recent developments," Appl. Energ. 170, 250-268 (2016).

[4] F. Crotogino, K. Mohmeyer, and R. Scharf, "Huntorf CAES: More than 20 Years of Successful Operation," Spring 2001 Meeting, Solution Mining Research Institute (2001).

[5] R. Swanekamp, "McIntosh serves as model for compressed - air energy storage," Power 12(2) 35-41 (2000).

[6] S. Mei, T. Zhang, X. Zhang et al., "Research and engineering practice of non-supplementary combustion compressed air energy storage: Taking Jintan national demonstration project as an example," Experimental Technology and Management 39(5) 1-8 (2022).

[7] Y. Mazloum, H. Sayah and M. Nemer, "Comparative Study of Various Constant-Pressure Compressed Air Energy Storage Systems Based on Energy and Exergy Analysis," J. Energ. Resour. 143(5) (2021).

[8] A. Sciacovelli, Y. Li, H. Chen et al., "Dynamic simulation of Adiabatic Compressed Air Energy Storage (A-CAES) plant with integrated thermal storage - Link between components performance and plant performance," Appl. Energ. 185, 16-28 (2017).

[9] H. Mozayeni, X. Wang and M. Negnevitsky, "Dynamic analysis of a low-temperature Adiabatic Compressed Air Energy Storage system," J. Clean Prod. 276, 124323 (2020).

[10] H. Guo, J. Xu, H. Chen et al., "Analysis of the efficiency of a AA-CAES system operating at a constant pressure," Journal of Engineering for Thermal Energy and Power 28(05), 540-546 (2013).

[11] X. Wen, S. Liu, X. Li et al., "Simulation and efficiency analysis of advanced compressed air energy storage system," Journal of Chinese Society of Power Engineering 41(9), 802-808 (2021).

[12] Z. Han, Q. Zhou, Y. Wang et al., "Analysis of two sorts of configurations of AA-CAES system," Acta Energiae Solaris Sinica 37(03), 629-635 (2016).

[13] A.G. Olabi, T. Wilberforce, M. Ramadan et al., "Compressed air energy storage systems: Components and operating parameters - A review," Journal of Energy Storage (2020).

[14] C. Guo, Y. Xu, H. Guo et al., "Comprehensive exergy analysis of the dynamic process of compressed air energy storage system with low-temperature thermal energy storage," Appl. Therm. Eng. 147, 684-693 (2019).

[15] T. Wang, G. Chai, X. Cen et al., "Safe distance between debrining tubing inlet and sediment in a gas storage salt cavern," J. Petrol. Sci. Eng. 196, 107707 (2021).

[16] D. Wu, J. Wang, B. Hu et al., "A coupled thermo-hydro-mechanical model for evaluating air leakage from an unlined compressed air energy storage cavern," Renew. Energ. 146, 907-920 (2020).

[17] X. Zhuang, R. Huang, C. Liang et al., "A coupled thermo-hydro-mechanical model of jointed hard rock for compressed air energy storage," Math. Probl. Eng. 2014, 169-179 (2014).

[18] X. Chen and J. Wang, "Stability analysis for compressed air energy storage cavern with initial excavation damage zone in an abandoned mining tunnel," Journal of Energy Storage 45, 103725 (2022).

[19] Y. Han, H. Ma, C. Yang et al., "The mechanical behavior of rock salt under different confining pressure unloading rates during compressed air energy storage (CAES)," J. Petrol. Sci. Eng. 196, 107676 (2021).

[20] J. Schön, "Physical Properties of Rocks: Fundamentals and Principles of Petrophysics," Pergamon 18, 333-348 (1998).

[21] M. Yan, M. Zhao, J. Li et al., "Thermodynamic analysis of cavern-type underground gas storage," Gas & heat 35(2), B01-B07 (2015).